

Performance analysis and optimization of a box-hull wave energy converter concept

Article

Accepted Version

Creative Commons: Attribution-Noncommercial-No Derivative Works 4.0

Bódai, T. and Srinil, N. (2015) Performance analysis and optimization of a box-hull wave energy converter concept. *Renewable Energy*, 81. pp. 551-565. ISSN 0960-1481 doi: <https://doi.org/10.1016/j.renene.2015.03.040> Available at <https://centaur.reading.ac.uk/73381/>

It is advisable to refer to the publisher's version if you intend to cite from the work. See [Guidance on citing](#).

Published version at: <http://dx.doi.org/10.1016/j.renene.2015.03.040>

To link to this article DOI: <http://dx.doi.org/10.1016/j.renene.2015.03.040>

Publisher: Elsevier

All outputs in CentAUR are protected by Intellectual Property Rights law, including copyright law. Copyright and IPR is retained by the creators or other copyright holders. Terms and conditions for use of this material are defined in the [End User Agreement](#).

www.reading.ac.uk/centaur

CentAUR

Central Archive at the University of Reading

Reading's research outputs online

Performance analysis and optimization of a box-hull wave energy converter concept

Tamás Bódai^{a,*}, Narakorn Srinil^b

^a*Meteorological Institute, University of Hamburg, Hamburg, Germany*

^b*Department of Naval Architecture, Ocean and Marine Engineering, University of Strathclyde, Glasgow, UK*

Abstract

In this paper we consider a wave energy converter concept which is created by linking a box barge to the mechanical reference by linear dampers. The response to incident wave action in terms of power take-off is expressed explicitly as the solution of a linear frequency-domain model. The simplicity of the model combined with the possibility of the application of theory allows for a nested, and so manageable, procedure of optimization. We find that for any geometry, i.e., a combination of e.g. the breadth-to-length and breadth-to-draught aspect ratios of the box, the optimum is characterized by resonance at least in one of the two degrees of freedom, heave or pitch. Furthermore, optimal geometries turn out to be extremal: either long attenuator-type or wide terminator-type devices perform the best. We find also that optimal wavelengths, which are comparable to the device length in case of attenuators, emerge either due to the progressively increasing buoyancy restoring force characteristic, or due to the finite bandwidth of irregular waves. In particular, diffraction forces are more significant under optimal conditions for performance in irregular seas in comparison with conditions necessary for the most intensive displacement response of the free-floating box barge exposed to regular waves.

Keywords: wave energy converter, optimization, box barge, radiation-diffraction analysis, dimensional analysis

1. Introduction

For economic viability the optimization of wave energy converters (WEC) has to satisfy extreme requirements [1, 2]. It has been recognized to be a difficult task in comparison with other types of renewable energy. For the survival and ultimate success of the industry it needs a higher degree of knowledge sharing at this early stage. Furthermore, in creating a knowledge base for the industry, beyond the examples of individual devices with their

*Corresponding author

Email addresses: `tamas.bodai@uni-hamburg.de` (Tamás Bódai), `narakorn.srinil@strath.ac.uk` (Narakorn Srinil)

31 ‘development narratives’, aspects of general interest should be considered too. Such fun-
32 damental aspects and the related theoretical analysis in most cases require abstraction and
33 simplification.

34 This paper presents a procedure for the optimization of an archetypal concept. A sketch
35 of the concept can be seen in Fig. 1, which also depicts the level of realism at which we
36 intend to address the problem of optimization. The floating part of the device concept is a
37 *large* box barge, whose free-floating motion was previously studied by Kraemer [3] with a
38 focus on the combined effects of wave frequency and wavelength. He made an attempt to find
39 optimal values of these, corresponding to the most intensive response, relative to the natural
40 frequency and device length, respectively. Outstanding questions remain, however, whether
41 the maximal amplitude of oscillation in pitch entails maximal power take-off (PTO) when
42 the PTO mechanism is represented very simply by a linear damper, and if the conditions
43 of optimum remain the same when varying other geometrical parameters that determine
44 performance.

45 In our study we are concerned with what can be viewed as the preliminary steps of
46 the development process of a WEC. We confine our analysis to the simple settings of small
47 amplitude 2-dimensional long-crested waves of an idealized frequency spectrum. We take the
48 most idealized picture of a PTO mechanism, a linear damper of constant characteristics, i.e.,
49 no PTO control is considered. However, studies considering PTO control [4, 5, 6, 7, 8, 9, 10]
50 show a promising potential for enhancing performance. Furthermore, the very simple box
51 hull-shape has been chosen in favor of the possibility of having a theoretical understanding.
52 A mooring system would also be inevitable for a working engineering construction in many
53 cases [11, 12]; and the list of further engineering compromises, which could impact strongly
54 on performance, could be continued. Furthermore we note that this study takes a point of
55 view that optimal design and environmental parameters together are searched for, with a
56 view of subsequently finding suitable sea sites for a device. The alternative would be to first
57 make a choice of a certain sea site, and then optimize the design parameters only, so as they
58 best suit that environment [13]. That is, we extend the settings defined by Kraemer mainly
59 by two components: (i) adding a PTO mechanism, and (ii) considering a wave spectrum.

60 A link of the float with the mechanical reference (i.e., Earth’s inertial frame of reference)
61 is an ideal choice in that – if given the same hull geometry – no other PTO mechanism is
62 expected to outperform this one. In a 2-dimensional (2D) setting, when the float is confined
63 to moving in a vertical plane only, the regular wave frequency and the damping coefficients of
64 a 2 degrees-of-freedom (2-DOF) device can be set so that the incident waves are completely
65 destructed, i.e., a 100% efficiency is theoretically possible [14, 15]. This possibility has been
66 recognized and experimentally demonstrated in case of other devices, such as: Salter’s duck
67 [16] and the Bristol cylinder [17]. If a link with the mechanical reference is not possible
68 and power take-off has to rely on inertial forces, a modified PTO mechanism is expected
69 to perform less effectively. In this case, however, one may adopt the following strategy to
70 find an optimum. One can retain the geometry that was found optimal having a link with
71 the mechanical reference, and then the objective is to tune the new PTO mechanism –
72 possibly involving inertial parts – in a way that it best mimics the effect of the ideal PTO
73 mechanism [18]. These ideas might apply in case of the free-floating SEAREV device [8].

Optimization, that is, finding the maximum value of an objective function, can be difficult in practice for various reasons. One reason may be that multiple local optima exist, in which case with different initial guess values for the parameters to be tuned, different and possibly misleading results can be obtained. Another reason may be that the objective function cannot be resolved smoothly numerically, which could challenge many optimization algorithms. Any such difficulties are enhanced by larger number of variables to be optimized. In this case, if various types of algorithmic or automatic optimum searches fail or provide inconsistent results, the manual treatment (as well as the troubleshooting) might be beyond the possibilities. Even if an algorithmic search terminates successfully, the interpretation is not necessarily possible without seeing the ‘context’ of the optimum, say, in a chart in which suboptimal regimes are presented as well. As for the presently considered WEC concept a combination of algorithmic and manual methods were applied successfully. By applying the method of dimensional analysis [19] we could not reduce the number of variables to be optimized, but, instead, by applying the so-called amplitude criterion of optimum [14] we could do just that; and, due to the simplicity of the model the response could be expressed explicitly, which greatly enhanced the efficiency of the numerics. The results of these procedures reveal that, indeed, the optimal solution is not unique, but long attenuator-type and wide terminator-type devices perform equally well. Furthermore, the dimensional analysis framework – if not for the envisaged purpose – could be utilized for the physical interpretation of the results.

The structure of the paper is as follows. In Sec. 2 a detailed mechanical model of the concept is given, including the equations of motion and the way irregular waves are accounted for. In Sec. 3 we review previous analysis of a free-floating box barge conducted in a nondimensional framework, and attempt the application of such methods to our WEC concept, which process sheds light on a possible method of optimization. In Sec. 4 we present results, and subsequently in Sec. 5 we discuss these results – providing some details of the optimization, and giving a physical interpretation of the results. In Sec. 6 we summarize our findings and draw conclusions.

2. Mathematical model

Mechanical model. The mechanical model of the box hull wave energy converter concept is shown in Fig. 1. Its details are explained as follows. The hull is a rectangular solid block, whose geometry is characterized by its breadth, draught, and length (B, D, L). There are two active degrees of freedom: a translational one in the vertical direction, heave (z), and a rotational one, pitch (φ). The corresponding constraints are symbolized in the sketch by a hinge, which is confined to moving in a vertical slide. In equilibrium the hinge always coincides with the still water level. This is a choice made in order to simplify the forthcoming analysis. The density of the hull is such that it is partially submerged, and the state of hydrostatic equilibrium is stable. The density, together with the geometry, determines the mass and inertia (m, θ). The elevation of the center of gravity (COG) is variable, but within limits of meeting the condition of hydrostatic stability. The effect of buoyancy is modeled mechanically by a linear spring characterized by a stiffness s_h , which links the mass with the

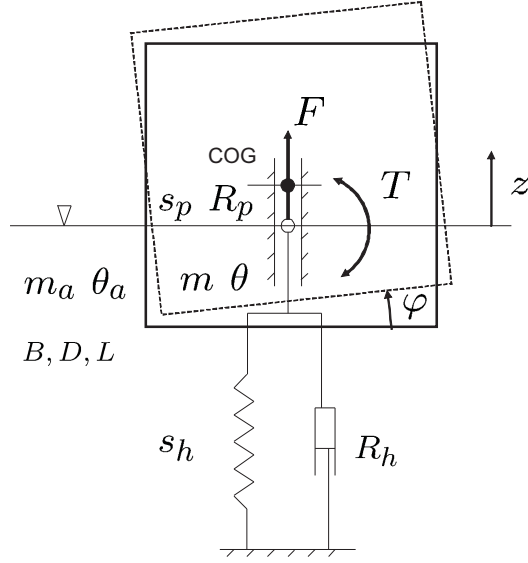


Figure 1: Mechanical model of the box-hull wave energy converter concept. The box barge, linked with the mechanical reference by dampers, oscillates in heave and pitch.

115 mechanical reference. In pitch, the spring is a torsional spring (s_p , graphically not indicated
 116 in the sketch). In either DOF a damping effect is accounted for as well, characterized by
 117 damping coefficients R_h and R_p , which are due to the radiation of waves when the float
 118 oscillates, entailing a loss of energy. A conjugate effect to this is that the moving body
 119 experiences an apparent increase of its mass and inertia as well (m_a, θ_a). This is commonly
 120 referred to as the added mass effect. The hydrodynamic damping and added mass effect
 121 are frequency-dependent [20, 15, 21, 14]. PTO in either DOF is achieved by linear dampers
 122 (k_h, k_p) connected in parallel with those that represent radiation damping (graphically not
 123 indicated in the sketch). That is, the PTO relies upon the mechanical reference. Due to
 124 wave action on the hull, there is a forcing of motion in the respective DOF's (F, T). We
 125 shall use 2D, i.e., long-crested waves throughout this analysis, which travel along the length
 126 of the barge.

127 *Governing equations and response.* The equation of motion in the frequency domain can
 128 be written in a matrix form:

$$[(i\omega)^2(\mathbf{M}_0 + \mathbf{M}_a) + i\omega(\mathbf{K} + \mathbf{R}) + \mathbf{S}]\mathbf{x} = \mathbf{Q}, \quad (1)$$

129 in which $\mathbf{x} = (z, \varphi)$ and $\mathbf{Q} = (F, T)$ are frequency dependent (phased) complex quantities; i is
 130 the imaginary unit; \mathbf{M}_0 and \mathbf{K} are diagonal matrices of structural mass and (PTO) damping,
 131 respectively. This formulation is unchanged when considering all six DOF's of the rigid body,
 132 which is our starting point in the determination of \mathbf{M}_0 and \mathbf{K} as for the 2-DOF model. For
 133 the definition of the displacement, we consider the one point of the rigid body which is the
 134 intersection of its vertical center line and the axis of the hinge. The frequency-dependent
 135 radiation-diffraction parameters of eq. (1), the added mass (\mathbf{M}_a), radiation damping (\mathbf{R}),

and force coefficients (\mathbf{Q} , including Froud-Krylov and diffraction forces), are in fact not independent [14]. For our analysis they are obtained by using the ANSYS AQWA software package (AQWA-LINE suite), which implements a boundary element method algorithm [22].

For the presently considered geometry and configuration, \mathbf{M}_a and \mathbf{R} in 6-DOF show the same pattern with regard to their nonzero entries (\cdot):

$$\begin{bmatrix} \cdot & 0 & 0 & 0 & \cdot & 0 \\ 0 & \cdot & 0 & \cdot & 0 & 0 \\ 0 & 0 & \cdot & 0 & 0 & 0 \\ 0 & \cdot & 0 & \cdot & 0 & 0 \\ \cdot & 0 & 0 & 0 & \cdot & 0 \\ 0 & 0 & 0 & 0 & 0 & \cdot \end{bmatrix}$$

These matrices are also symmetric. On the other hand, the stiffness matrix \mathbf{S} has diagonal nonzero entries only. These imply that heave is an independent DOF. Considering also that the hinge moves in a vertical slide, which can be modeled with infinite stiffness in sway, pitch is the only other active DOF remaining. Thus, the two active DOF's are independent. Consequently, the solution in either DOF can be given explicitly (with the example of heave) as follows:

$$z = \frac{F}{-\omega^2(m + m_a) + i\omega(k_h + R_h) + s_h}. \quad (2)$$

The force coefficient f provided by AQWA is defined as the force for unit wave amplitude: $F = F_{e,3} = fA$. With this, the mean power take-off, that is, the rate of energy conversion on the linear damper, is:

$$P_h = k_h(\omega|z|)^2/2; \quad (3)$$

and likewise in pitch.

In the independent DOF of heave the time-domain equation of motion assumes the following form:

$$\begin{aligned} & [m + m_a(\infty)]\ddot{z}(t) + k_h\dot{z}(t) \\ & + k_{r,h}(t) * \dot{z}(t) + s_h z(t) \\ & = f(t) * a(t). \end{aligned} \quad (4)$$

This is a linear integro-differential equation, in which the asterisk $*$ denotes the operation of convolution; and the impulse response function is defined [14] as:

$$k_{r,h}(t) = 2\mathcal{F}^{-1}[R_h(\omega)]. \quad (5)$$

In the above, \mathcal{F}^{-1} denotes the operation of (inverse) Fourier transformation. The frequency-dependent force vector $f(\omega)$ is similarly transformed into the time domain (but without a 2

157 times multiplier); and for a regular wave the amplitude of water surface elevation in some
 158 reference position is:

$$a(t) = A \sin(\omega t). \quad (6)$$

159 Time-domain equations for general 3D scenarios can be generated and solved using the
 160 AQWA-NAUT program suite. By doing so we can validate the above reconstructed 1-DOF
 161 frequency-domain equations of motion and subsequently obtained solutions. AQWA-NAUT
 162 recalculates the Froud-Krylov forces in every time step considering finite displacements and
 163 finite wave heights, i.e., nonlinear effects. Therefore, in order to validate linear equations,
 164 small wave heights have to be used. This is done in Appendix A.

165 *Hydrostatic stability.* Denoting the elevation of the COG by z_g (positive upward), the
 166 structural inertia of a rectangular solid is calculated as:

$$\theta = \frac{1}{12}m[L^2 + 4(D + z_g)^2] + mz_g^2; \quad (7)$$

167 and the stiffness in pitch is expressed as:

$$s_p = s_{p0} - mgz_g. \quad (8)$$

168 In the latter s_{p0} is the stiffness if the COG coincides with the hinge. Notice that when z_g is
 169 positive, the stiffness is decreasing according to an inverted pendulum effect. On the other
 170 hand, the inertia is always greater for a nonzero z_g . The stiffness and the inertia determines
 171 the natural frequency (squared):

$$\alpha_p^2 = \frac{s_p}{(\theta + \theta_a)}. \quad (9)$$

172 For some values of z_g the box can capsize, however, and its upper and lower critical values
 173 need to be identified.

174 The following formula provides a connection between the elevation of COG and the
 175 density of float:

$$z_g = D \left(\frac{\rho_w}{2\rho} - 1 \right). \quad (10)$$

176 For hydrostatic stability in pitch it is required that the metacentric height be positive [23]:

$$GM = BM - BG > 0, \quad (11)$$

177 where

$$BM = I/V. \quad (12)$$

178 In the above, the metacenter (M) and the elevation of the COG (G) are given relative to
 179 the point of attack of the integrated buoyancy force ($z_B = -D/2$); I is the second moment

of inertia of the water plane area with respect to the x -axis; and $V = BDL$ is the displaced (water) volume. In terms of the design parameters, criterion (11) takes the following form:

$$z_g < \frac{(L/2)^2}{3D} - \frac{D}{2}, \quad (13)$$

which provides an upper bound on z_g . A lower bound is determined by the condition of preventing complete immersion:

$$-D/2 < z_g, \quad (14)$$

which is equivalent to requiring $\rho < \rho_w$.

Wave spectrum. Up to this point we have considered regular waves only. As we detail it in the next section, regular waves do not in fact yield an optimum when using the linear model, and the resonance effect is also not ‘robust’ when considering irregular waves. Since in reality sea waves are never regular, already in this preliminary analysis we consider irregular waves of some finite bandwidth. For our purposes it will suffice to use a simple symmetric model spectrum, $S(f)$ ($\omega = 2\pi f$), which is referred to as the water surface elevation spectrum. We define this spectrum using the functional form of the probability density of the standard normal distribution of mean μ and variance σ^2 (with no physical meaning intended): $\phi(x) = \frac{1}{\sqrt{2\pi\sigma^2}} \exp[-(x - \mu)^2/(2\sigma^2)]$. It is a suitable choice given that it is normalized so that $\int_{-\infty}^{\infty} \phi(x)dx = 1$. In order to specify S , we define the significant wave height H_s in terms of the zeroth moment of the spectrum, $m_0 = \int_0^{\infty} S(f)df$, such as: $H_s = 4\sqrt{m_0}$ [24]. We note that since the lower boundary of the integral for m_0 is not $-\infty$ but 0, there is a small error using $\phi(x)$. Collecting the formulas above, the wave spectrum is written in full as:

$$S(f) = \left(\frac{H_s}{4}\right)^2 \times \frac{1}{\sqrt{2\pi\sigma^2}} \exp[-(f - f_0)^2/(2\sigma^2)], \quad (15)$$

in which f_0 [s^{-1}] is the peak frequency; and σ [s^{-1}] can be regarded as a bandwidth parameter. In our analysis we use narrowband waves ($\sigma = 0.05$) which grant us the benefit of having a physical meaning of the results in most of the considered parameter regime; whereas using more realistic broadband spectra, like e.g. Pierson-Moskowitz or JONSWAP, would render the physical meaning in some regimes.

Mean power take-off. In frequency domain the power spectrum of an actual response can be obtained simply from the synthesis of the power spectrum corresponding to (over the frequency range uniformly) unit wave amplitudes, $P_1 = P_h(A = 1) + P_p(A = 1)$ [Wm^{-2}] using e.g. eqs. (2) and (3), and the actual water surface elevation spectrum, $S(f)$ [m^2s], [25]:

$$P(f) = 2P_1(f)S(f); \quad (16)$$

209 from which the overall mean PTO is:

$$\bar{P} = \int_0^{\infty} P(f)df. \quad (17)$$

210 In numerical calculations the power (3) and wave spectra (15) are discretized [$S_i = S(f_i)$];
 211 and thus the integral (17) is replaced by a sum, the number of terms in which are limited
 212 by a (reasonably chosen) maximal cut-off frequency.

213 3. Rationale and methods of analysis

214 *Free-floating box barge.* Prior to the main analysis in this paper we attempted to recon-
 215 struct Kraemer’s results [3] regarding a free-floating box barge, lacking any power take-off
 216 mechanism or external damping. The methodology and parameters of our reconstruction
 217 are as follows. The box barge is assumed to be halfway submerged. Furthermore, we fixed
 218 $L = 20$ and $V = BDL = 640$, and varied B and D jointly, and varied ω as well. The
 219 frequency ω is sampled fine enough so that very narrow-banded resonance peaks could be
 220 resolved. Sample values for D , which would imply values for B , are chosen such as: $2D = 4,$
 221 $6, 8, 10, 10.8, 11.2, 12, 12.5$. The fixed regular wave height is: $H = 0.1$. Note that $H = 2A$.
 222 The reconstructed results are displayed in Fig. 2. The oscillation amplitude in pitch as a
 223 function of the frequency ratio ($\pi_1 = \omega/\alpha_p$) and the wavelength ratio ($\pi_4 = \lambda/L$) is plotted.
 224 In the latter the wavelength of a regular wave of frequency ω in deep water is:

$$\lambda = 2\pi g/\omega^2. \quad (18)$$

225 The independent variables π_1 and π_4 are nondimensional, which are varied via dimensional
 226 ones, B and ω . It can be shown that the considered problem can be described in terms of
 227 either four independent dimensional or four nondimensional variables. (We will detail such
 228 an analysis shortly as for the complete WEC model described in Sec. 2.) The remaining
 229 two nondimensional variables – held constant in Fig. 2 – can be defined as $\pi_3 = V/H^3$, the
 230 nondimensionalized volume, and $\pi_2 = BD/H^2$, a constraint on the aspect ratios. Results are
 231 reconstructed using a linear frequency-domain model [Fig. 2 (a)], as well as a nonlinear time-
 232 domain model [Fig. 2 (b)]. Notice the different physical units for the oscillation amplitude
 233 associated with the two diagrams, and also that in panel (a) the range of the frequency ratio
 234 ω/α_p shown is much shorter in order to resolve very narrow-banded resonance peaks.

235 The fact that the linear model deviates greatly from the nonlinear model for larger
 236 wavelength ratios indicates that the former is not valid. The oscillation amplitudes that
 237 can be read off of the diagram in Fig. 2 (a) are certainly not realistic. However, for small
 238 oscillation amplitudes and wave heights the two models agree well, as demonstrated in
 239 Appendix A (in case of the externally damped structure, to be introduced shortly below).
 240 The diagram in Fig. 2 (b) corresponding to the nonlinear model reveals a pair of optimal
 241 frequency ratio and wavelength ratio:

$$\pi_1 = \omega/\alpha_p \approx 1 \quad \text{and} \quad \pi_4 = \lambda/L \approx 5. \quad (19)$$

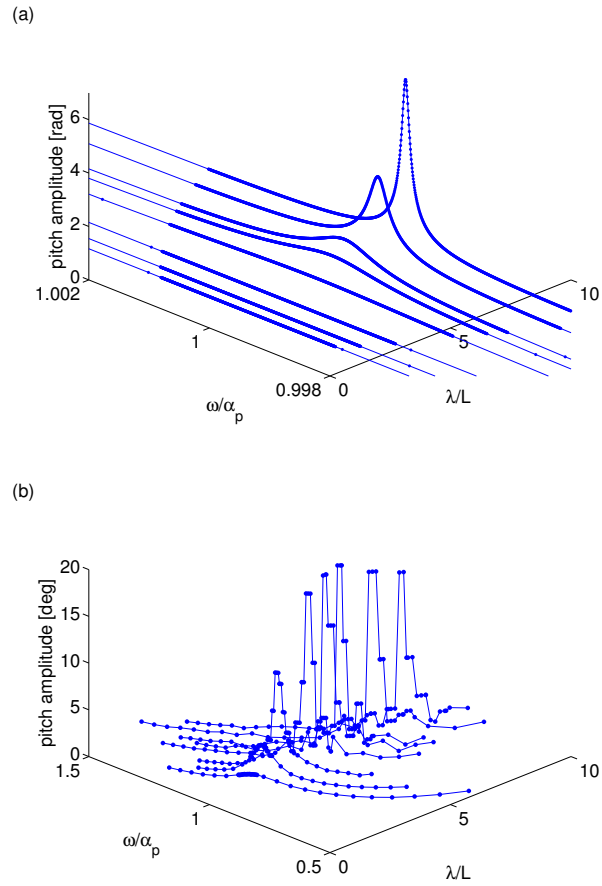


Figure 2: Oscillation amplitude of a free-floating box barge in pitch as a function of the frequency ratio (π_1) and the wavelength ratio (π_4), using (a) a frequency-domain and (b) a time-domain model. Sampling of the response is indicated by markers. In both cases we fixed $L = 20$ and $V = 640$; and a series of draught values were set, such as: $2D = 4, 6, 8, 10, 10.8, 11.2, 12, 12.5$. The wave height in both cases is: $H = 0.1$. Notice the different physical units as for the oscillation amplitude.

242 Such an optimum is due to the progressively increasing, i.e., *nonlinear*, restoring buoyancy
 243 force characteristic deriving from the hull shape. With regard to the wave frequency, on
 244 the other hand, the optimum corresponds to resonance – as expected from the theory of
 245 WECs [14]. The linear model does not in fact admit an optimal wavelength ratio, but it
 246 yields ever-increasing oscillation amplitude and decreasing response bandwidth. This effect
 247 is discussed in more detail in Appendix B. The oscillation amplitude is in fact very closely
 248 related to the inverse of the bandwidth, and they are *progressively* increasing. This is a
 249 feature of our results based on the linear model which disagree – for a yet unidentified
 250 reason – with the results reported by Kraemer based, apparently, also on a linear model:
 251 Kraemer reported a *degressive* increase and a seemingly unaffected bandwidth, with no
 252 indication of the behavior beyond the range of wavelength ratios examined (0-5). Apart
 253 from this, based on our results we conclude that a linear model in the present setting is not
 254 suitable to predict the optimum, as it is outwith the range of model validity.

255 *Power take-off by dampers.* As a step further, the model described in Sec. 2 can be
 256 obtained by linking the box hull to the mechanical reference by dampers. Next, the frame-
 257 work of analysis used in case of the free-floating box barge is applied to the WEC with the
 258 dampers. Now the objective function of optimization is the power. The objective of this
 259 exercise is to see if the conditions for optimum (19) hold. The following setup is picked for
 260 this analysis. The barge is assumed to be halfway submerged, that is, its COG lies on the
 261 axis of hinge. The fixed size of the barge is: $\rho_w V = 2 \cdot 10^5$ kg. The breadth is set to be
 262 $B = 5$, and a series of draughts are considered, such as: $D = 2.2, 2.4, 2.6, 2.8, 3, 3.1, 3.2,$
 263 $3.25, 3.3, 3.35, 3.4, 3.425, 3.45, 3.475, 3.5, 3.525$. With this, the definition of $\pi_2 = BD/H^2$ is
 264 modified to $\pi_2 = LD/H^2$. However, this makes no difference in the interpretation. Using a
 265 linear model, whose results are shown in Fig. 3 (a), a condition for optimum in terms of λ/L
 266 does not exist, the amplitude is increasing and the bandwidth is decreasing monotonically
 267 – very much alike the displacement response of the free floating barge.

268 Introducing irregular waves [Fig. 3 (b)], with a nonzero bandwidth of the wave spectrum,
 269 an optimal value of λ/L emerges, which is about 2. It is significantly smaller than 5 under
 270 (19), owing to the larger bandwidths of the response at smaller values of the wavelength
 271 ratio. That is, the conditions for optimum (19) do not hold. We conclude thus that besides
 272 nonlinear effects, irregular waves are also found to be able to render very high amplitude
 273 responses and to create an optimum. Furthermore, the diffraction forces are more signifi-
 274 cant under the conditions of optimal performance in irregular seas in comparison with the
 275 conditions necessary for the most intensive displacement response of the free-floating barge
 276 exposed to regular waves.

277 A further important conclusion to draw is that with finite bandwidth irregular waves
 278 the response stays in the linear regime, and so we can make the favorable choice of using
 279 the linear frequency-domain model for our optimization procedure, which requires much less
 280 numerical effort when calculating the response in comparison with the use of the (nonlinear)
 281 time-domain model.

282 *Dimensional analysis.* In order to have a direction for pursuing optimization, a complete
 283 dimensional analysis of the WEC is given next. It is outlined in Table 1. According to
 284 the standard procedure [19] on the left hand side of the table listed are all the dimensional

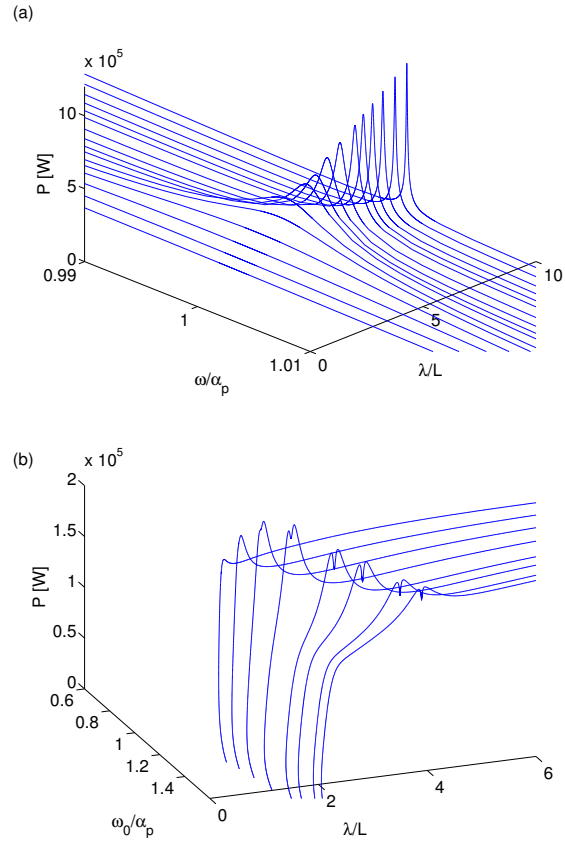


Figure 3: (a) The total power take-off (PTO) of a box barge as a function of the frequency ratio (π_1) and the wavelength ratio (π_4). We fixed $\rho_w V = 2 \cdot 10^5$ kg and $B = 5$; and a series of draught values are considered such as: $D = 2.2, 2.4, 2.6, 2.8, 3, 3.1, 3.2, 3.25, 3.3, 3.35, 3.4, 3.425, 3.45, 3.475, 3.5, 3.525$. (b) The total PTO (with the first few sample values of D as listed above) achieved when using irregular waves. (Instead of ω we write ω_0 , the peak frequency of the frequency spectrum.)

Table 1: Outline of dimensional analysis

Dimensional variables	Physical unit	Nondimensional variables
ω_0 , peak frequency	$(\text{rad}\cdot)\text{s}^{-1}$	$\pi_1 = \omega_0/\alpha_p$
B , breadth	m	$\pi_2 = \omega_0/\alpha_h$
D , draught	m	$\pi_3 = BDL/H_s^3$
L , length	m	$\pi_4 = \lambda_0/L$
ρ , density of barge	$\text{kg}\cdot\text{m}^{-3}$	$\pi_5 = \rho/\rho_w$
k_h , damping in heave	$\text{kg}\cdot\text{s}^{-1}$	$\pi_6 = k_h/ Z_{i,h}(\omega_0) $
k_p , torsional * in pitch	$\text{kg}\cdot\text{m}^2\cdot(\text{rad}^{-1}\cdot)\text{s}^{-1}$	$\pi_7 = k_p/ Z_{i,p}(\omega_0) $
ρ_w , water density	$\text{kg}\cdot\text{m}^{-3}$	
g , gravitational acceleration	$\text{m}\cdot\text{s}^{-2}$	
H_s , significant wave height	m	
P , power	$\text{kg}\cdot\text{m}^2\cdot\text{s}^{-3}$	$\pi_0 = P/P_{ref}$

Table 2: Account of dimensional analysis

Number of p 's	$n = 10$
Number of fixed p 's	$n_F = 3$
Number of dimensionally independent p 's	$k = 3$
Number of dimensionally independent fixed p 's	$k_F = 3$

285 parameters (p 's) that determine the objective function, the power P . These include design
286 parameters, B , D , L , ρ , k_h , k_p , environmental parameters, f_0 , H_s , and also global param-
287 eters, $\rho_w = 1024.4 \text{ kg/m}^3$, $g = 9.807 \text{ m/s}^2$. The latter three are fixed in this analysis. All
288 these parameters together constitute a complete set, i.e., they uniquely define the problem
289 (e.g. the way we need to do so for computations using ANSYS AQWA) and the solution.
290 Applying Buckingham's π theorem [19], modified for the case when some p 's are fixed, the
291 number of independent π 's that fully describe the problem is:

$$N = (n - k) - (n_F - k_F) = 7. \quad (20)$$

292 which is not fewer than the $(n - n_F)$ dimensional variables. For an account of the dimensional
293 analysis see Table 2. Thus, the dimensional analysis could not reduce the dimensionality or
294 order of the problem, and so optimization cannot be simplified in this way. On the right
295 hand side of Table 1, accordingly, we list a complete set of nondimensional variables (π 's).
296 In there P_{ref} is an arbitrary reference power level; and the intrinsic impedance (with the
297 example of heave) is defined as:

$$Z_{i,h} = i\omega(m + m_a) + R_h + s_h/(i\omega). \quad (21)$$

298 The π 's are defined not in a conventional way but so that they can provide a physical
299 meaning of an optimal solution, and possibly facilitate the application of some criteria of
300 optimum, based on theory or perhaps experience. This could open up another way of
301 utilizing dimensional analysis in order to reduce the dimensionality of the problem. It is

straightforward to show that in case of a 1-DOF (2D or 3D) linear oscillatory system maximal PTO is achieved by setting:

$$k = |Z_i| \quad (22)$$

at any¹ frequency. This setting is to satisfy the amplitude criterion of optimum. In our case it dictates that $\pi_6 = 1!$ and $\pi_7 = 1!$ (Note that we denote by the exclamation mark a ‘requirement’ for a certain objective (optimum here), as in variational calculus. The exclamation does not denote here the factorial of a nonnegative integer.) With 1-DOF a complementary criterion for optimum is the phase criterion, which requires that the excitation force (the sum of Froude-Krylov and diffraction forces) be in phase with the velocity of oscillation, which is in fact satisfied in resonance [14]. One might think that in our case the phase criterion dictates that either $\pi_1 = 1!$ or $\pi_2 = 1!$ However, it makes no immediate contradiction proposing that the optimum might poses itself as a ‘compromise’, in which case there is no perfect resonance in any of the DOF’s; or in other words: one can assume that the optimum occurs when $\pi_1 \neq 1$ and $\pi_2 \neq 1$ simultaneously. Certainly, resonance in both DOF’s in the same time can be satisfied² only in special cases. Since in case of our 2-DOF and 3D WEC there are other variables too that determine optimum, it is unlikely that the ultimate optimum would occur in that special situation. One of the further variables is the device size, π_3 , which we will fix³. Another one is the wavelength ratio, for which – as demonstrated above – we do not have a universally applicable rule of optimal setting. There is also no trivially optimal setting as for the density ratio π_5 .

Customized framework of optimization. With the application of some criteria of optimum, and also directly fixing the size π_3 , the dimensionality of the problem could be reduced in principle. In practice, however, no advance has been made, because the mapping between the p ’s and π ’s involves the computationally expensive diffraction analysis. Therefore, our approach is to pursue optimization in terms of the dimensional parameters, and then translate the results into terms of the nondimensional ones for the purpose of interpretation, in order to see, for example, if optimum entails resonance.

In general the optimization is increasingly more complicated with the increasing number of variables. In our case, however, owing to the simplicity of the mathematical model and the applicability of theory, the procedure of optimization can be broken down into subsequent manageable stages as follows.

- (i) As our starting point, in accordance with the first column of Table 1 we write the objective function, the power take-off, as a function of the dimensional design parameters and the one environmental parameter, the (peak) frequency, with respect to which there is a nontrivial optimum:

$$P_{(i)}(\omega_0, B, D, L, \rho, k_h, k_p).$$

¹The amplitude criterion is usually formulated assuming that resonance takes place already [$k = R(\omega = \alpha)!$], which is a special case of eq. (22).

²With regular waves in a 2D setting, this is the condition for the total destruction or stopping of the incident waves, which results in 100% efficiency.

³For finding an economic optimum, the size that determines costs has to be varied subsequently.

337 We can separate the parameters into two groups by a semicolon such that on its left we
 338 write the variables with respect to which we are looking for the optimum, and on its right
 339 we write the variables whose value we fix.

340 **(ii)** Although we are interested in finding an optimum with respect to B and D , we will
 341 search for this optimum – or, give a representation of the dependence of P on them –
 342 visually, and so we write B and D immediately right to the semicolon:

343
$$P_{(ii)}(\omega_0, L, \rho, k_h, k_p; B, D).$$

344 In order to *eliminate* variables from the left of the semicolon,

345 **(iii)** first the size $V = BDL$ is fixed, which – having fixed B and D – amounts to fixing L ,
 346 and so we write:

347
$$P_{(iii)}(\omega_0, \rho, k_h, k_p; B, D, V).$$

348 So given a fixed geometry, the diffraction analysis can be carried out for a range of frequencies
 349 ω .

350 **(iv)** The density ρ can be varied via varying z_g [more precisely $\rho = \rho(z_g, D)$; see eq. (10)],
 351 which takes its effect through the *analytically* given response [see eqs. (2), (3), (7),
 352 (8), (9)].

353
$$P_{(iv)}(\omega_0, z_g, k_h, k_p; B, D, V)$$

354 **(v)** The damping coefficients are set according to eq. (22) in a straightforward manner
 355 to produce P_1 , but substituting ω_0 for ω in that equation before applying eq. (16):

356
$$k_{h/p} = k_{h/p}(\omega_0, B, D, V, \rho).$$

357
$$P_{(v)}(\omega_0, z_g; B, D, V)$$

358 **(vi)** Finally the optimum with respect to ω_0 and z_g can be found by a nested procedure:
 359 we solve the equation

360
$$P'_{(v),z_g}(\omega_0(z_g), z_g; B, D, V) = 0$$

361 in which $\omega_0(z_g)$ is found by solving $P'_{(v),\omega_0}(\omega_0; z_g, B, D, V) = 0$

362 Regarding $P_{(v)}(\omega_0; z_g, B, D, V)$ involved in the latter, refer to Fig. 11 (b) for a visual clue,
 363 where slices of the analytically given function $P_{(v)}(\omega_0, z_g; \cdot)$ at various fixed values of z_g can
 364 be seen.

365 The feasibility of our method is due in large part to the fact that we have to look for the
 366 maximum of functions of a *single* variable at a time. We achieved this by using Matlab's
 367 function `fmincon`, which implements a constrained optimum search algorithm. This way
 368 the optimal power (with fixed device size) can be mapped out as a function of B and D to
 369 yield a chart, which is easy to represent and interpret, and facilitates the ultimate purpose
 370 of indicating the optimal geometry.

371 We note that in order to nondimensionalize the objective function P , we used an arbitrary
 372 reference power level P_{ref} . A more meaningful way to nondimensionalize P would be dividing
 373 by the power in the incident waves in a window which is equal with the width of the WEC,
 374 P_w [26]. This nondimensional quantity is called the relative capture width:

$$\text{RCW} = P/P_w, \quad (23)$$

in which

$$P_w = \frac{\rho_w g^2}{64\pi} H_s^2 T_e B. \quad (24)$$

This quantity is a mean value. In the definition T_e is the energy period, which will be approximated as $2\pi/\omega_0$, because the wave spectrum to be used is narrow-banded. In general, however, the energy period of an irregular wave is different from its zero mean crossing period (T_z): $T_e = m_{-1}/m_0$ and $T_z = m_0/m_2$ [26]. T_e can be interpreted as the wave period of a regular wave (of equal significant wave height $H_s = \sqrt{2}H$) which carries the same energy as the irregular wave in question. We note that for the spectrum defined above m_{-1} cannot be obtained analytically. Although more meaningful, the RCW is not so useful as the objective function of optimization, because it is the power itself which has to be maximal, which does not necessarily occur under the same conditions as the maximal RCW. Nevertheless, we will provide a chart of the RCW too, because it can indicate if the results are realistic/correct or not. For example, for a wide ($B \gg D, L$) terminator-type device, exposed to irregular waves, $\text{RCW} < 1$ can only be realistic, even under optimal conditions. As for a long ($L \gg B, D$) attenuator-type device, $\text{RCW} \gg 1$ is possible, while it would not necessarily outperform a terminator-type device of the same size (V).

4. Results

In this section we present optimal figures for the objective function of optimization, the power take-off P , and of the variables ω_0 and z_g , i.e., the dependent and independent variables of $P_{(v)}(\omega_0, z_g; \cdot)$. Optimal figures for some derived variables defined previously are also shown. The results are presented in terms of color charts showing the various quantities mapped out in terms of the geometric parameters B and D . In terms of point (iii) of the previous section the mass of device is fixed to be: $\pi_3 H_s^3 \rho_w = 2 \cdot 10^5$ kg. Lower bounds on the geometric parameters are imposed such as: $B_{min} = 2$, $D_{min} = 1$, $L_{min} = 2$. An upper bound on D is independently imposed ($D_{max} = 10$), because of uninteresting features for larger values of it. Within their respective ranges, B and D are sampled with increments of 2 and 0.2 m, respectively, and the cartesian product of the resulting sets of sample values is taken to sample the B - D plane. Sample values which do not satisfy that $L > L_{min}$ are ignored; i.e., the considered domain of the B - D plane is bounded by the graph of a reciprocal function. For all relevant computations whose results are presented in this section the significant wave height is fixed to be $H_s = 2\sqrt{2}$. This is to establish equivalence in an approximate sense with a regular wave of unit amplitude, considering that rather *narrow-banded* irregular waves are used ($\sigma = 0.05$).

In Fig. 4 color charts of power in heave (c), (d), pitch (e), (f), and their sum (a), (b), are displayed. Color bars are included to indicate the magnitude of power for the various (B, D) scenarios. For certain scenarios we have coexisting local optima. Diagrams on the left (right) correspond to results when the optima are due to resonance in pitch (heave).

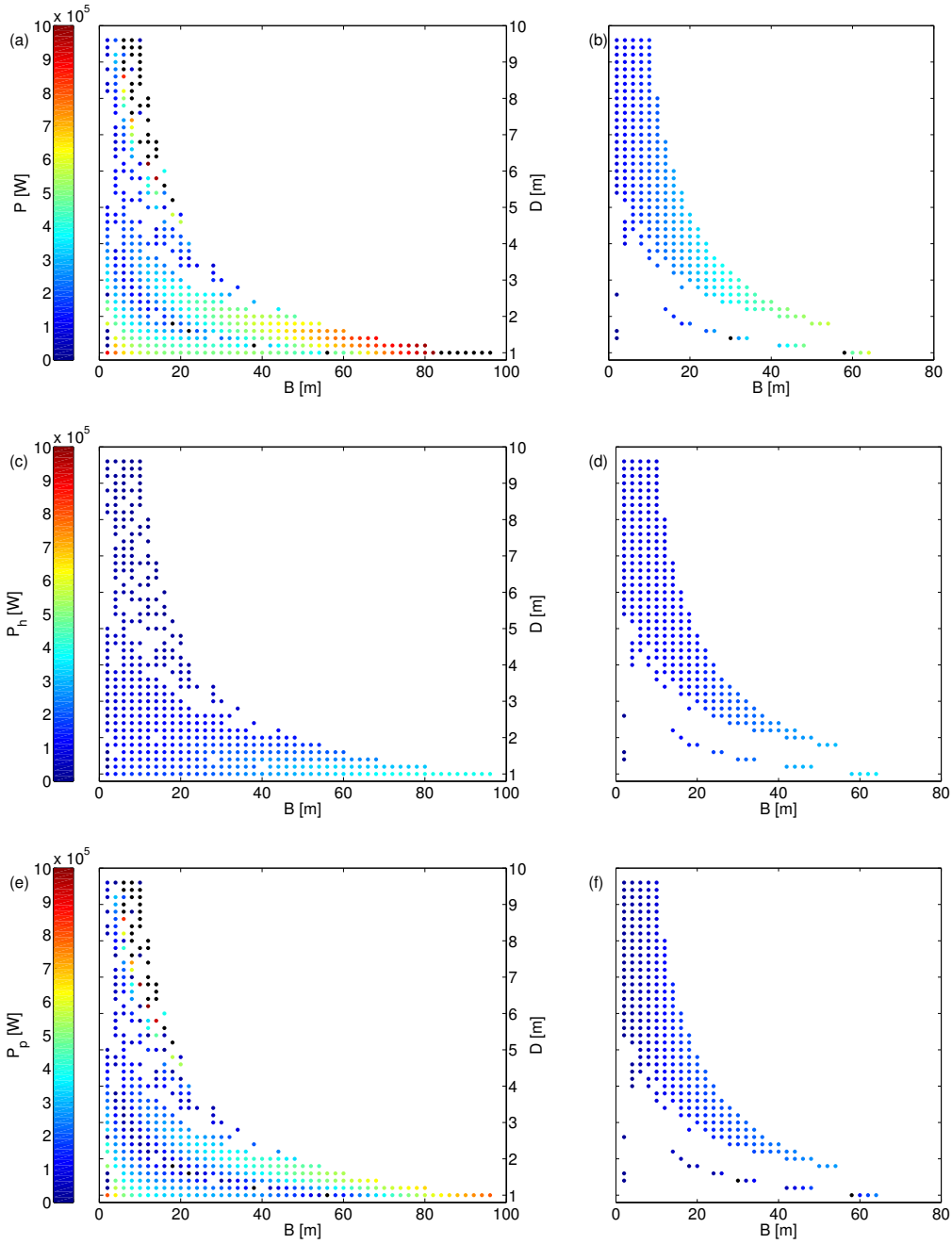


Figure 4: Power take-off in pitch (e), (f), heave (c), (d), and the sum of these (a), (b), depending on geometric parameters of the box hull, the breadth B and draught D . Diagrams on the left (right) [e.g. (a) ((b))] correspond to results when optima are due to resonance in pitch (heave). A significant wave height of $H_s = 2\sqrt{2}$ was used. For other settings for the simulations, refer to the main text. (An overbar is not used here to denote *mean* power in Watts.)

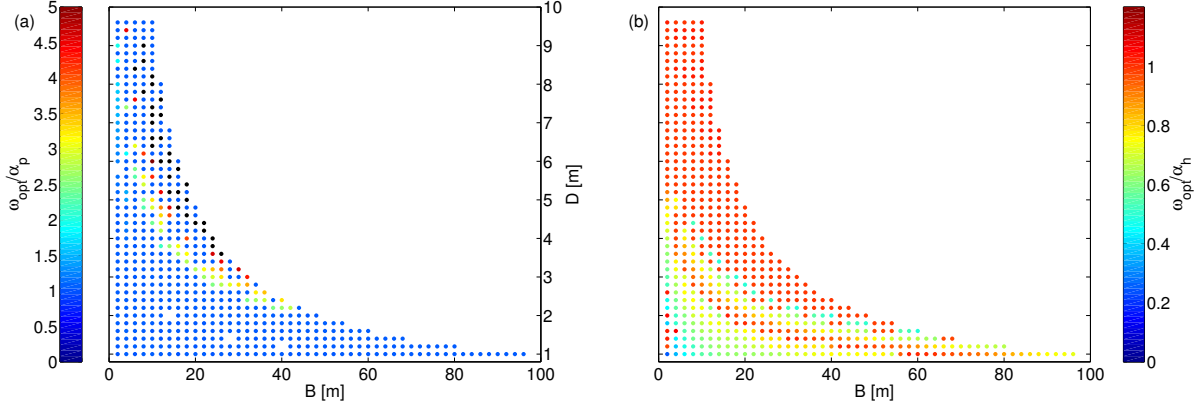


Figure 5: Frequency ratio corresponding to data that Fig. 4 was produced from.

Figure 5 indicates whether the optimum (the better performing one when there are two local optima) is due to a resonance in pitch or heave with the appropriate frequency ratio being nearly unity. For the construction of this figure natural frequencies were calculated using eq. (9), and optimal (peak) frequencies (shown in Fig. 6), along with optimal z_g 's (shown in Fig. 7) (or optimal π'_5s), were found using Matlab function `fmincon` (as described in point (vi) in the previous section). Two initial guess values (IV) were set such as: $\omega_0 = \alpha_p$ and $\omega_0 = \alpha_h$, with $z_g = z_{min}$ in both cases. With this setting, when there is only one optimum, i.e., when a single resonance peak exists, the solution converges to the unique optimum using either IV. Regarding the subsequent optimum search for z_g , since the surface that represents the power take-off over the plane of ω_0 - z_g features a ridge (which ridge represents resonance; see Fig. 11 (b)), the arbitrary choice for the IV's $z_g = z_{min}$ should suffice. Note that in order to ensure the accuracy of calculating the power through eqs. (16) and (17), ω has to be sampled sufficiently for the purpose of resolving even extremely narrow-banded responses due to resonance.

For all the color charts in this section (except those of $z_{min,max}$ and $\omega_{opt}/\alpha_p(h)$) some data points are missing, because either `fmincon` did not terminate successfully or the correctness of data was dubious. The condition to filter them out was set as follows:

$$|\omega_{opt}/\alpha_p(h) - 1| < 0.03.$$

As mentioned above, it can happen that there are two distinct (coexisting) peaks of resonance in pitch and heave. In this case the charts would overlap, and so we chose not to present them in one diagram, but rather separately: the chart corresponding to resonance in pitch (heave) on the left (right). Charts of the wavelength ratio (π_4) and RCW are displayed in Fig. 8 and Fig. 9, respectively. In Fig. 7 and elsewhere black markers are used when the value is greater than the subjectively chosen upper limit to be indicated by colors (see the color bars). This approach was taken for the reason that 'outliers' did not carry valuable information, and their inclusion in the range of the color bar would result in poor visual

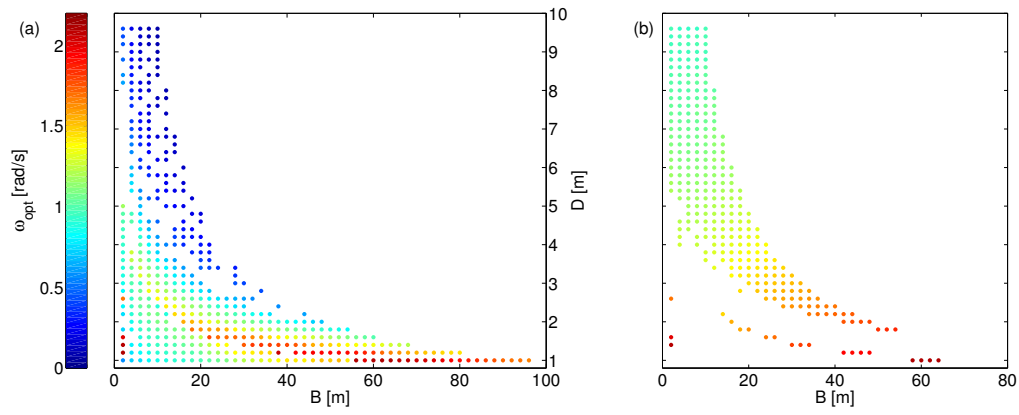


Figure 6: Optimal (peak) frequency corresponding to data that Fig. 4 was produced from.

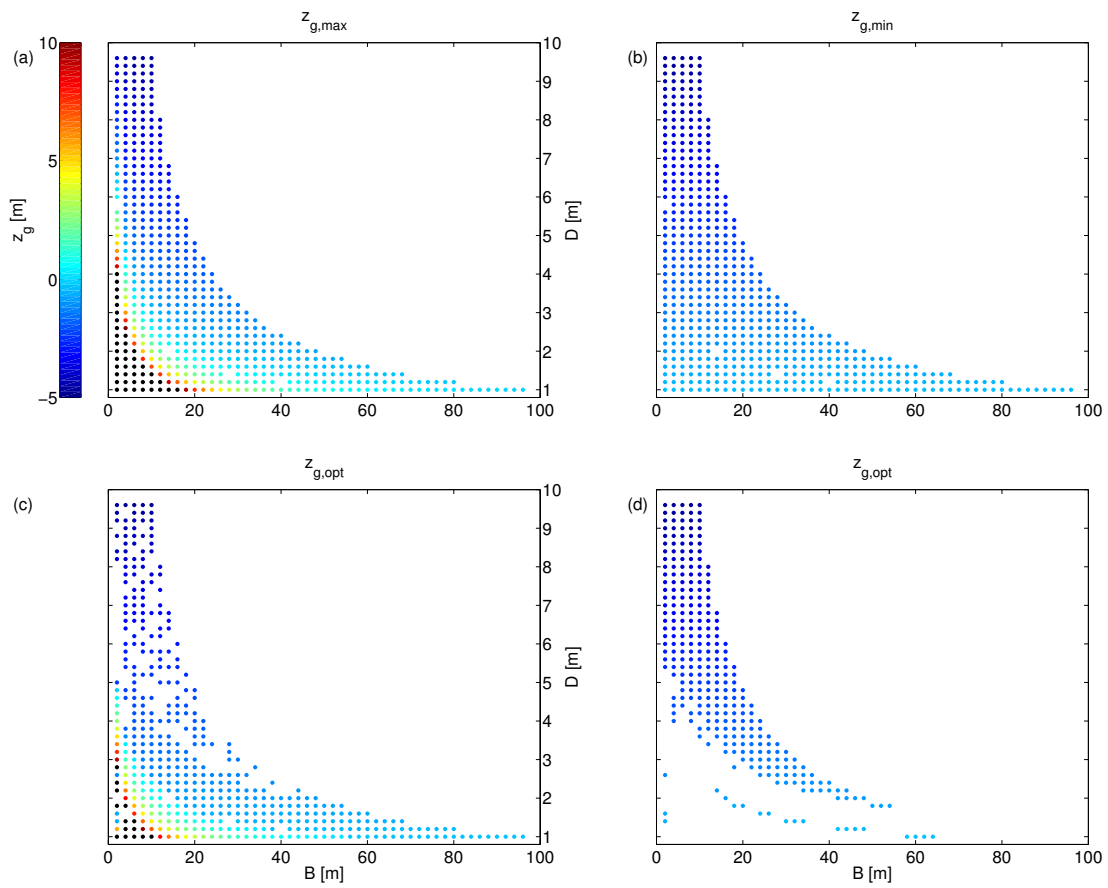


Figure 7: Upper (a) and lower (b) boundaries for the elevation of the COG, and its optimal values (c), (d).

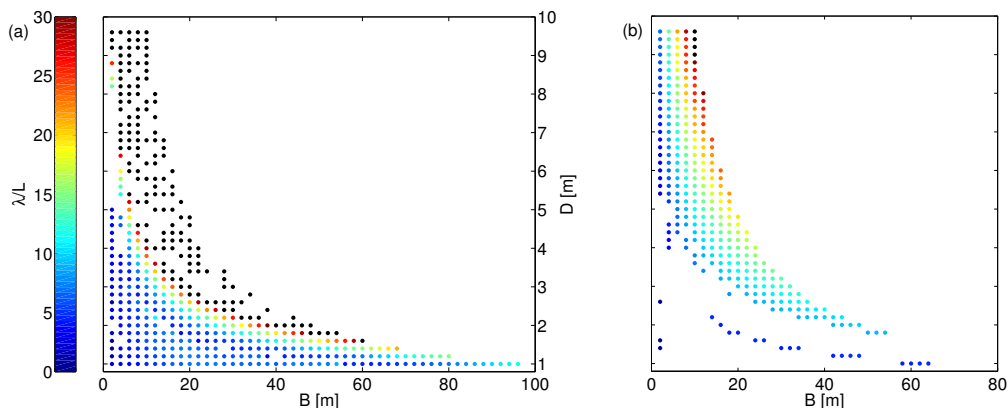


Figure 8: Wave length ratio corresponding to data that Fig. 4 was produced from.

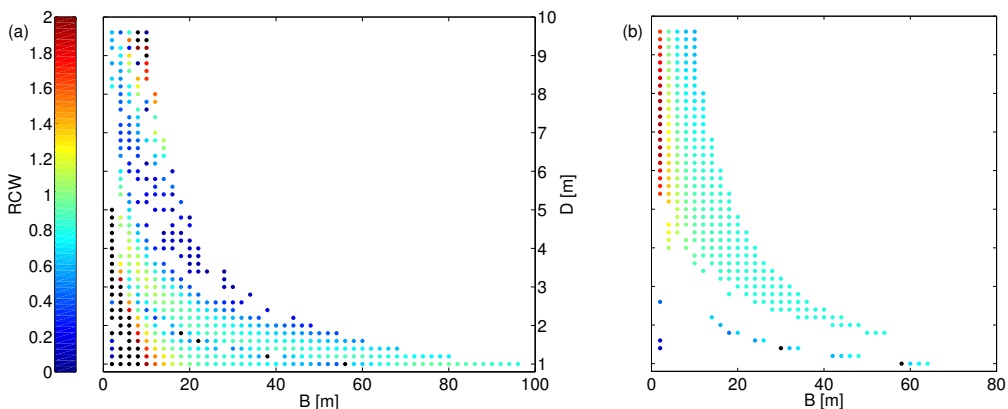


Figure 9: Relative capture width corresponding to data that Fig. 4 was produced from.

resolution of other features of interest.

436

5. Discussion

437

5.1. Optimum approximately in resonance

438

Relating Fig. 5 to Fig. 4 it can be said that maximal PTO (for any fixed B and D) is due to resonance, at least in one of the two DOF's, because at least on of the frequency ratios approximates unity closely. (However, it is important that the frequency ratios are not exactly unity, as we explain this in Sec. 5.4.) The resonance peak is preserved even if the total power $P = P_h + P_p$ from heave and pitch is considered. The response in heave shows no interesting features: P changes monotonically with B or D ; thus, features of the total PTO are inherited from pitch. (We demonstrate some behavior of the system that gives rise to this feature in Sec. 5.5.) However, it does not mean that heave is less productive. It is

439

440

441

442

443

444

445

446

447 possible that $P_p (h) > P_h (p)$ while $\pi_1 (2) \gg 1$ or $\pi_1 (2) \ll 1$ and $\pi_2 (1) \approx 1$. For both of the
 448 latter two points an illustration is provided by the individual of $(B, D) = (20, 4.8)$, in which
 449 case resonance occurs in heave, and pitch slightly outperforms heave [cf. Fig. 4 (d) and (f)].

450 Comparing e.g. Figs. 6 (a) ((b)) and 4 (e) ((d)), features of the color charts for power
 451 are clearly related to that of the natural frequency. In heave, with decreasing D the water
 452 plane area and so the stiffness increase, which increases the natural frequency. In pitch, the
 453 geometry determines the natural frequency in a nontrivial manner. Since the optimum is
 454 due to resonance, the performance the better the *wave* frequency the lower, as indicated by
 455 eq. (24).

456 5.2. Hydrostatic stability

457 Regarding the lower bounds on z_g [Fig. 7 (b)], it is a simple inclined flat surface according
 458 to eq. (14). As for the upper bound [Fig. 7 (a)], it is rapidly growing for large L 's according
 459 to eq. (13). Its excessively large values we chose not to resolve in the chart, because very
 460 high elevations of the COG are not practical, as it requires the density of the float to be
 461 very small. Nevertheless, the power is evaluated in accordance with the excessively large
 462 values of z_g . Clearly, imposing a smaller upper limit on z_g would reduce the power. The
 463 optimal values of z_g are searched for using `fmincon` within the limits implied by eqs. (14)
 464 and (13). When resonance occurs in heave, the lower limit is found always optimal [Fig.
 465 7 (d)], and there is a departure from this at a certain point, already in the regime when
 466 resonance occurs in pitch [Fig. 7 (c)].

467 Figures 7 (a) and (b) prompt that very often the optimal z_g is bracketed very tightly
 468 by its limiting values. Under such circumstances if the device oscillates, it is expected that
 469 – even if the requirements of hydrostatic stability are met – it may capsize. The critical
 470 wave height for capsizing can also be rather small. To prevent the WEC from capsizing a
 471 ballast or a keel to the lowermost point of the float can be installed. As an extension of
 472 the present analysis, the keel could be modeled as a concentrated point mass, with which
 473 the distribution of mass is nonuniform. The overall structural density would increase, and
 474 the device ballasted down would immerse deeper. The ratio of the mass of ballast and float
 475 could be a further nondimensional variable that the performance depends on, which would
 476 make the problem of optimization more complicated. In fact, the purpose of introducing
 477 variability in the density of the float was nothing but to maintain stability in case of any
 478 (B, D) scenario; now, however, this solution turns out to be not always sufficient.

479 5.3. Elevation of the COG impacting on the response bandwidth

480 In our preliminary analysis using regular waves, in connection with Fig. 3, z_g was not
 481 optimized for, but held fixed at $z_g = 0$. Some individuals featured in our analysis, subjected
 482 to appropriately narrow-banded irregular waves, turned out to have a *nontrivial* optimal z_g ,
 483 however. In Fig. 10 featuring the individual of $D = 2$ exposed to *regular* waves the effects
 484 of the increasing elevation of the COG is shown, resulting in: increasing response amplitude
 485 and decreasing bandwidth. For any particular $z_g > 0$, through the inverted pendulum effect
 486 the natural frequency is smaller, at which frequency, for a fixed geometry, the frequency-
 487 dependent damping is also smaller, and in the same time the excitation torque is greater.

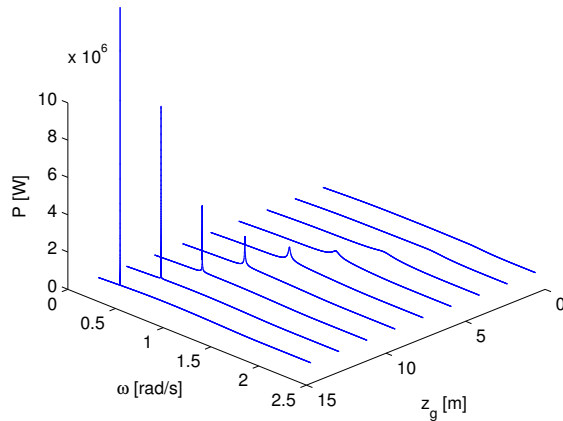


Figure 10: Total power take-off depending on the wave frequency and the elevation of the COG, for the individual $(B, D, L) = (5, 2, 20)$. The regular wave height was set to be: $H = 2$.

5.4. Optimum slightly off-resonant

488

A similar situation to the latter is shown in Fig. 11 (a) for a wide ($B = 30$) terminator-type WEC. Using *irregular* waves [see panel (b) of that figure] the lower limit for z_g is found to be optimal, because the bandwidth of response is decreasing for the increasing elevation of the COG. For this optimal value, $z_{g,min}$, the response as a function of the frequency is reproduced in Fig. 12 (a). In the same diagram, for a comparison of the bandwidths, the spectrum of irregular waves is also shown (in green) with an arbitrary peak frequency. (The spectral ordinates $S(\omega)$ are scaled up appropriately in order to be able to present the spectrum in the diagram of $P(\omega_0)$.) As a gross feature the response is double-peaked; one peak corresponds with resonance in pitch (left), and another one with resonance in heave (right), the latter being a much more broadbanded effect. On a more detailed level, it can be seen that the peak corresponding to the resonance in pitch is double-peaked itself. The reason for this is the following. Figure 12 (b) shows the absolute value of the intrinsic impedance in pitch, $|Z_{i,p}|$, which is the optimal choice for the external damping k_p . It has a minimum value for the resonant frequency (which minimum value is not zero, just orders of magnitude smaller than the optimal k_p well away from the resonant frequency). The bandwidth of the response P_1 depends on the impedance or damping (see Appendix B). Thus, the response P_1 is the most narrow-banded in resonance, and even though its ordinates just off resonance are smaller, the bandwidth is larger, and so the synthesized response P with the use of irregular waves, according to eq. (16), can feature larger ordinates just off resonance.

489

490

491

492

493

494

495

496

497

498

499

500

501

502

503

504

505

506

507

508

5.5. Nonmonotonic dependence of the power take-off in pitch

509

For the geometry in question the excitation torque is also shown in Fig. 13, which is to indicate that its magnitude depends on the frequency, and it has a characteristic maximum at some point. This scenario is chosen from a ridge of the total power showcased in Fig. 4

510

511

512

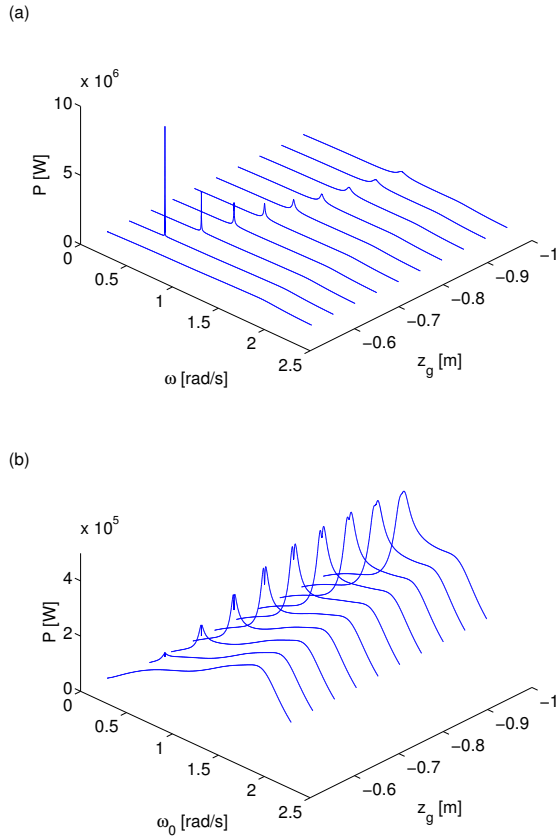


Figure 11: Total power take-off depending on the wave frequency and the elevation of the COG, for the individual $(B, D, L) = (3, 2, 3.2539)$, with regular waves of $H = 2$ (a) and irregular waves of $H_s = 2\sqrt{2}$ (b).

513 (a) or (e) (corresponding to the maximum of power as a function of D for each fixed B).
 514 It is pointed out that for $D = 2$ the maximum of the excitation torque does not coincide
 515 with the resonance peak of the response P . A maximum of P at $D = 2$ occurs such that for
 516 smaller values of D it is the magnitude of excitation that is decreasing, and for larger values
 517 of D , it is the resonant or natural frequency that is decreasing. For lower frequencies the
 518 magnitudes of excitation is smaller, even though its peak value is further increasing with D .

519 5.6. Different characteristics of optimal power and RCW

520 Similarly as with the power, the RCW also features a ridge [Fig. 9 (a)], but it does not
 521 coincide with that of the power. Instead, it seems to align with a curve in the B - D plane
 522 defined by $\pi_1 = \pi_2 = 1$ (see Fig. 5), i.e., when resonance occurs in the two DOF's in the
 523 same time. (A strip closely confined to this curve shows up in isolation in the right hand side
 524 of all color charts.) This offset of the ridges is notable; it arises now because the frequency is
 525 a variable to be optimized for. On the ridge of the RCW the resonant frequencies in heave
 526 and pitch are equal, which value is greater than the optimal one. The lower-frequency wave

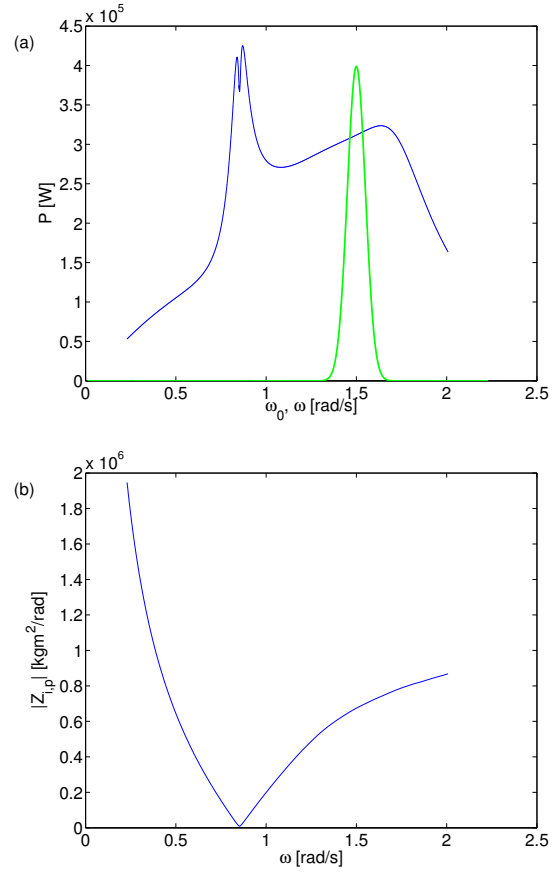


Figure 12: Showcase of an individual from the ridge of the surface of the total power take-off (PTO) seen in Fig. 4: $(B, D, L) = (3, 2, 3.2539)$. (a) Frequency response in terms of the total PTO. For reference, we included in the same diagram the model spectrum of irregular waves (thick green line) of an arbitrary peak frequency (ordinates are suitably scaled to fit the diagram). The irregular wave height is set as: $H_s = 2\sqrt{2}$; and $z_g = -0.8$ m. (b) Absolute value of the intrinsic impedance, which is not zero but has a minimum at resonance.

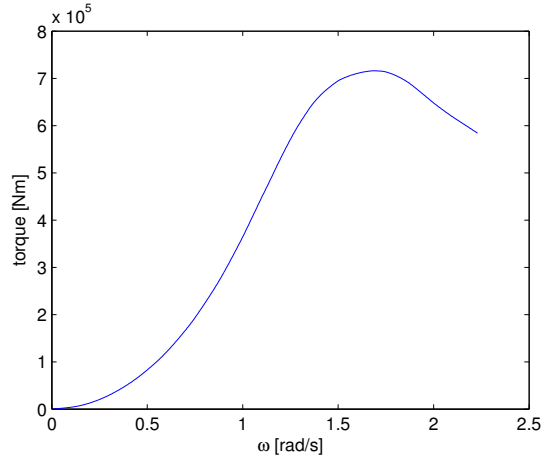


Figure 13: A follow up of Fig. 12: frequency dependent excitation torque in pitch.

527 carries more energy, and even if a smaller percentage is harnessed, the total performance
 528 can still be better. That is, interestingly, resonance in only one of the DOF's can be better
 529 than resonance in both DOF's.

530 Consider resonance in pitch. The color in Fig. 9 (a) indicates that the RCW approaches
 531 unity from below for increasing B 's while fixing $L = L_{min}$. This is consistent with the
 532 fact that B is an increasing multiple of λ (see Fig. 8), that is, the 3D wave diffraction
 533 effects are more and more marginalized to the ends of the wide device, and so the situation
 534 is dominantly 2D. And since the situation is close to resonance in both DOF's, and the
 535 damping coefficients are set according to the amplitude criterion, we do indeed expect [14]
 536 that the incident waves are largely destructed. However, a full destruction of waves, even
 537 under the most favorable conditions, cannot happen, because of the finite bandwidth of the
 538 wave spectrum.

539 5.7. Optimal geometry

540 Reflecting on the performance characteristics of the concept (Fig. 4) we can say that
 541 optimal or well-performing individuals are found for extremal settings of the geometric
 542 parameters, which make either a very long barge head on the waves, an attenuator-type
 543 WEC, or a very long spine spanning as wide a window of the waves as possible, a terminator-
 544 type WEC. By changing the geometry in terms of B and D , moving away from these extremes
 545 is the 'least costly' along the paths of either minimal L or minimal B . Intermediate values
 546 of geometric parameters correspond to not so well-performing individuals.

547 5.8. Optimal wavelength

548 A realistic level of optimal performance can be associated with a very wide range of
 549 optimal wavelength ratios depending on the chosen geometry (Fig. 8); that is, in answer
 550 to an outstanding question concerning previous analysis: a universally applicable optimal

value cannot be identified. For better-performing longer attenuator-type WEC's, the optimal wavelength is comparable with the device length, being typically a few multiples of it.

It is emphasized once more that in our analysis the frequency is optimized for. It is consistent with an approach when first a well-performing WEC is designed, and then suitable wave sites are searched for. In the reverse direction a particular wave site has to be utilized and best accommodated, the environmental conditions are thus being given. This way the frequency is not a variable but fixed; or more realistically, instead of a single frequency value, a so-called wave scatter (wave height-wave period) matrix describing the conditions at the particular site is given. This may change the solution to the problem as provided by Fig. 4.

6. Summary and concluding remarks

In this paper we advanced previous *linear* time-domain analysis of a large box barge, which is exposed to significant wave diffraction forces when its dimension along the direction of wave propagation is comparable to the wavelength, i.e., when the *wavelength ratio* – a measure introduced to the analysis of wave energy converters (WEC) by Kraemer – is small. Kraemer reported, however, that, considering regular waves, in order to achieve larger response of the *free-floating* box barge in *pitch* (regarded favorable in case of WECs) the wavelength ratio does not need to be small or near unity, but can be much larger than that. Here we conducted a similar analysis using a *nonlinear* time-domain model, and found an optimal value of about five. Such an optimum emerges due to the progressively, i.e., nonlinearly, increasing buoyancy restoring force with increasing angular displacement and so oscillation amplitudes.

We found also another mechanism that can create an optimum: with increasing wavelength ratio the bandwidth of the transfer function is decreasing progressively, and so the WEC is increasingly incapable of responding to irregular waves. That is, with irregular waves (of moderate height) the oscillation amplitudes remain in the approximately linear regime. Therefore, also considering that calculations in the frequency-domain are much more straightforward and inexpensive, we preferred for our analysis to use linear frequency-domain models with irregular waves.

As the subject of our new and main analysis, we proposed a simple wave energy converter concept by adding dampers to the box barge in the degrees of freedom of pitch and heave, linking it to the mechanical reference. We showed that in a linear frequency-domain model these degrees of freedom *decouple*, and so the power take-off is made up of two independent parts. In this favorable case we were able to develop a customized method of optimum search, and to apply it successfully. For the *algorithmic optimization* of the wave frequency and the elevation of the center of gravity we exploited the simplicity of the model, which allowed us to derive the response analytically; and for the determination of the optimal values of the damping coefficients we applied theory, namely, the amplitude criterion of optimum. We conducted the optimum search in terms of dimensional variables, and then translated the results into terms of nondimensional variables for the purpose of *physical interpretation*: For any geometry, we found optimum approximately in *resonance*, occurring at least in one of the two degrees of freedom.

592 We have identified two geometrical parameters, the breadth and draught of the box barge,
593 with respect to which there is *no unique optimum* in the sense of a local maximum of the
594 power take-off occurring at some nontrivial intermediate value of any of the parameters. As
595 an algorithmic optimization procedure concerning the breadth and draught could not provide
596 immediately meaningful results, the dependence of the performance and other quantities on
597 these two parameters is provided here visually by color charts. The chart of the performance
598 revealed that better performing individuals have *extremal geometry*: it is either a long
599 attenuator-type device, or a wide terminator-type device, with dominant contribution from
600 pitch or heave, respectively. As for the former type, the optimal wavelength (deriving
601 from the optimal frequency) is comparable with the *optimal device length* (conditioned to
602 a fixed device size/displacement, and so restricted through the restrictions on D and B
603 imposing some minimal values on them) – typically a few multiples of it – and is shorter
604 if the bandwidth of the irregular wave frequency is broader. In this regard we note that
605 *diffraction* effects are more *significant* considering optimal performance in irregular seas
606 over the previously studied optimal – or, putting it more precisely: most intensive – motion
607 (damped only through wave radiation) due to regular waves.

608 We have also found that – similarly as with the wave length ratio described above – the
609 response amplitude (bandwidth) of the transfer function increases (decreases) monotonically
610 with the elevation of the center of gravity of the barge in the linear model with regular waves.
611 Again, this is rendered by either nonlinear progressive restoring forces or irregular waves.
612 Through these two mechanisms an *optimal elevation* can emerge.

613 Some remarks on the validity of the results produced by our simple model are due
614 here, however. Excessively large predicted optimal oscillation amplitudes and/or large wave
615 heights are *not consistent* with the linear diffraction analysis – apart from the fact that
616 nonlinear buoyancy forces are already accounted for. In this case performing simulations by
617 solving the fundamental equations of fluid mechanics or empirical model tests (in laboratory
618 or at sea) might be necessary.

619 Even if the oscillations are within the linear regime to a good approximation, they might
620 be still large enough that the device would *capsize*, which is an event that our frequency-
621 domain model cannot register. Having performed the optimization with the linear model,
622 therefore, a *reality check* must follow, e.g. using the time-domain model built in AQWA-
623 NAUT to check for the possibility of capsizing in the case of suspected individuals. It
624 is expected in general that theoretically optimal and robust operational conditions rarely
625 coincide, and a *compromise* has to be made. Nevertheless, linear models can be extremely
626 powerful as a guide for the optimum search, or, the search for viable concepts and individuals.

627 The much more difficult problem of finding an economic optimum has not been pursued
628 here. For this the costs have to be modeled in terms of the device size.

629 **Acknowledgements**

630 Facilities to carry out this research were provided by Green Ocean Energy Limited (UK);
631 it is gratefully acknowledged.

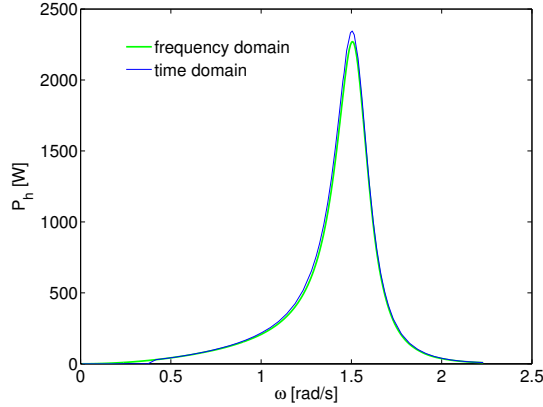


Figure A.14: Comparison of simulation results, in terms of the power generated in heave, for a frequency-domain and a time-domain model, using very small waves ($H = 0.1$). The scenario is described by the following: $(B, D, L) = (30, 3.2, 2.0337)$.

Appendix A. Agreement of the linear frequency-domain and nonlinear time-domain models 632 633

The validity of the linear model of our box-hulled WEC concept breaks down when excessively large amplitudes of excursion are predicted, typically in resonance. For small amplitude oscillations the linear model is accurate. Its predictions in terms of the power in heave are corroborated with the predictions of the nonlinear model, as shown in Fig. A.14. The regular wave height is set to be $H = 0.1$. The damping is held constant, at a value which is optimal for the resonant natural frequency. The time-domain model involves an arm of length $l_a = 50$ m, which, using very small waves, is approximately the same in effect as a vertical slide. For somewhat larger amplitudes the finite arm length has a strong effect on the performance both in heave and pitch (not shown here); and it also makes a significant difference if it is a leading or trailing arm (equivalent in effect with reversing the wave direction, also not shown). 634
635
636
637
638
639
640
641
642
643
644

Appendix B. Growing response amplitude with vanishing bandwidth 645

For a 1-DOF harmonic oscillator it is easy to show that the resonant velocity amplitude (u_{max}) can be expressed in terms of the amplitude of excitation force (F) and the damping (R , including internal and external damping) as follows: 646
647
648

$$u_{max} = F/R. \tag{B.1}$$

This relation is verified in case of the individuals considered in connection with Fig. 2 by evaluating terms on the left and right hand sides. Motion in the independent DOF of pitch is considered. On the one hand we obtained u by using the formula derived for the displacement response [analogous to (2)]. The displacement is multiplied by the frequency 649
650
651
652

653 ω to have velocity. Using discrete values of the frequency, with a sufficiently fine resolution,
654 the maximal velocity is selected. On the other hand we took the fraction of the force and
655 damping as obtained by radiation-diffraction analysis. Diagrams of the frequency-dependent
656 force coefficient and radiation damping are shown in Fig. B.15 (a) and (b), respectively.
657 The curves are coded by the same color as the markers on the horizontal axis that indicate
658 by their position on the axis the corresponding natural frequency. It can be seen that with
659 increasing draughts (device size fixed) the excitation torque is decreasing, and, on the other
660 hand, the radiation damping is decreasing at an even greater rate. This is true in terms of
661 either the peak values that these frequency-dependent functions take, or the values taken at
662 the natural frequencies. When the data obtained by the two alternative means are plotted
663 in the same diagram, Fig. B.16 (b) concerning the free-floating box barge, the agreement
664 appears to be exact. Thus, a monotonically growing response amplitude with variation in
665 the geometry is thereby accounted for.

666 In the same linear framework it is meaningful to define the bandwidth and relative
667 bandwidth [14], respectively, of a 1-DOF linear oscillatory system as follows:

$$\Delta\omega = R/m \quad (\text{B.2})$$

668 and

$$\Delta\omega/\alpha = R/\sqrt{sm}. \quad (\text{B.3})$$

669 The meaning of $\Delta\omega$ is a frequency range where the kinetic energy exceeds half of its maximal
670 value ($mu_{max}^2/4$); and α ‘refers to’ the resonant or natural frequency. The relative bandwidth
671 (which is the inverse of the nondimensional velocity amplitude) has been evaluated for the
672 considered individuals, and the resulting diagram is plotted in Fig. B.16 (a). Indeed, in
673 parallel with increasing (dimensional) amplitude, the bandwidth is vanishing. This, accounts
674 for our observations regarding Fig. 2 (a).

675 References

- 676 [1] Callaghan J. Future Marine Energy. Tech. Rep. CTC601; Carbon Trus; 2006. Available from:
677 www.carbontrust.co.uk.
- 678 [2] Falnes J. A review of wave-energy extraction. *Marine Structures* 2007;20(4):185 – 201.
- 679 [3] Kraemer DRB. The effect of wavelength on the response of floating ocean wave-energy conversion
680 devices. In: *Proceedings of the 7th European Wave and Tidal Energy Conference*. Porto, Portugal;
681 2007,.
- 682 [4] Iversen LC. Numerical method for computing the power absorbed by a phase-controlled point absorber.
683 *Applied Ocean Research* 1982;4(3):173 –80.
- 684 [5] Eidsmoen H. Optimum control of a floating wave-energy converter with restricted amplitude. *J Offshore
685 Mech Arct Eng* 1996;118:96–102.
- 686 [6] Korde UA. Latching control of deep water wave energy devices using an active reference. *Ocean
687 Engineering* 2002;29(11):1343 –55.
- 688 [7] Babarit A, Duclos G, Clment A. Comparison of latching control strategies for a heaving wave energy
689 device in random sea. *Applied Ocean Research* 2004;26(5):227 –38.
- 690 [8] Babarit A, Clément AH. Optimal latching control of a wave energy device in regular and irregular
691 waves. *Applied Ocean Research* 2006;28(2):77–91.

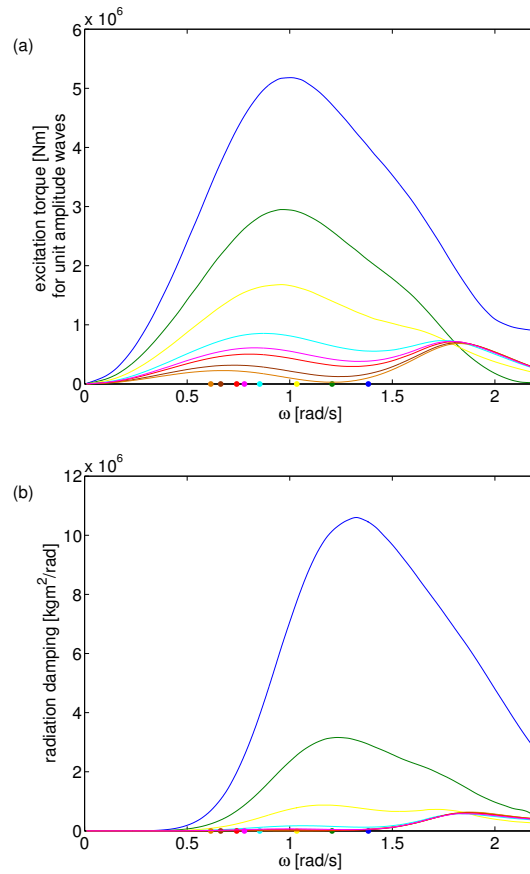


Figure B.15: Hydrodynamic parameters related to features of the diagrams seen in Fig. 2. In each diagram the same individuals are considered as in the said figure. The colored markers on the horizontal axis of frequency mark the values of the natural frequencies belonging to the curves of the respective hydrodynamic property each drawn in the same color as the marker. The markers from right to left in order correspond to the curves from top to bottom.

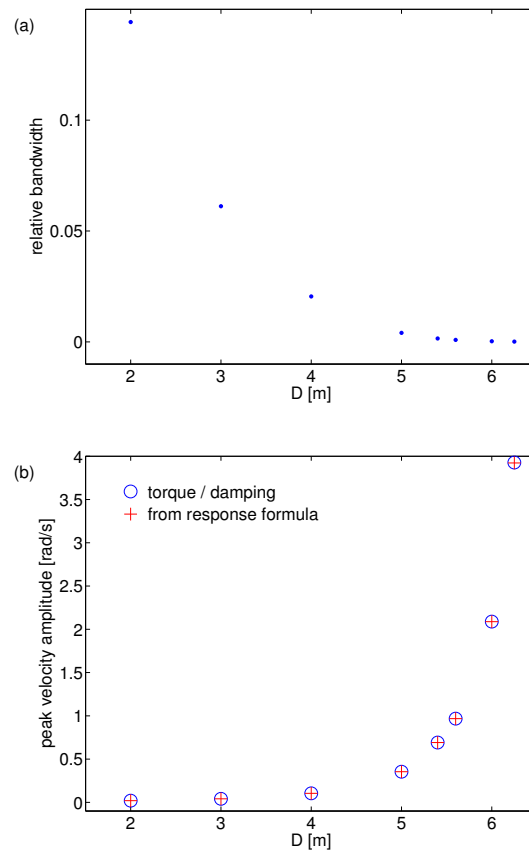


Figure B.16: A follow up of Fig. B.15. In each diagram the same individuals are considered as in the said figure. In panel (b) the cross marker shows values obtained by a response formula analogous to (2).

- [9] Kara F. Time domain prediction of power absorption from ocean waves with latching control. *Renewable Energy* 2010;35(2):423–34. 692
- [10] Hong Y, Waters R, Boström C, Eriksson M, Engström J, Leijon M. Review on electrical control strategies for wave energy converting systems. *Renewable and Sustainable Energy Reviews* 2014;31(0):329–42. 693
- [11] Cerveira F, Fonseca N, Pascoal R. Mooring system influence on the efficiency of wave energy converters. *International Journal of Marine Energy* 2013;3-4(0):65–81. 694
- [12] Zanuttigh B, Angelelli E, Kofoed JP. Effects of mooring systems on the performance of a wave activated body energy converter. *Renewable Energy* 2013;57(0):422–31. 695
- [13] Aurelien D, Babarit A, Clément AH. Optimizing the power take off of a wave energy converter with regard to the wave climate. *J Offshore Mech Arct Eng* 2005;128:56–64. 696
- [14] Falnes J. *Ocean waves and oscillating systems*. Cambridge University Press; 2002. 697
- [15] Evans DV. Power from water waves. *Annual Review of Fluid Mechanics* 1981;13(1):157–87. 698
- [16] Salter SH. Wave power. *Nature* 1974;249:720–4. 699
- [17] Evans DV, Jeffrey DC, Salter SH, Taylor JRM. Submerged cylinder wave energy device: theory and experiment. *Applied Ocean Research* 1979;1(1). 700
- [18] Korde U. On providing a reaction for efficient wave energy absorption by floating devices. *Applied Ocean Research* 1999;21(5):235–48. 701
- [19] Sonin AA. *The physical basis of dimensional analysis (Second Edition)*. Department of Mechanical Engineering, MIT, Cambridge, MA 02139; 2001. 702
- [20] Evans D. A theory for wave-power absorption by oscillating bodies. *Journal of Fluid Mechanics* 1976;77:1–25. 703
- [21] Count BM. On the dynamics of wave-power devices. *Proceedings of the Royal Society of London Series A, Mathematical and Physical Sciences* 1978;363(1715):559–79. 704
- [22] Garrison CJ. *Hydrodynamic Loading of Large Offshore Structures: Three-dimensional Distribution Methods*. Wiley; 1978,. 705
- [23] Kemp JF, Barrass CB, Young P. *Ship Stability: Notes and Examples*. Butterworth-Heinemann; third ed.; 2001. 706
- [24] Chakrabarti SK. *Hydrodynamics of Offshore Structures*. WIT Press; 1987. 707
- [25] Barltrop NDP. *Dynamics of Fixed Marine Structures*. Marine Technology Directorate Ltd.; 1991. 708
- [26] Tucker MJ, Pitt EG. *Waves in Ocean Engineering; vol. 5*. Elsevier, Kidlington, UK; 2001. 709
- 722